

Supporting Information

Trivalent Cerium Preponderant CeO₂/Graphene Sandwich-structured Nanocomposite with Greatly Enhanced Catalytic Activity for Oxygen Reduction Reaction

Yu Yu,^a Xiaofang Wang,^a Wenyu Gao,^a Pei Li,^a Wei Yan,^a Songmei Wu,^a Qihong Cui,^a Weiguo Song,^{*b} and Kejian Ding^{*b}

^a School of Science, Beijing Jiaotong University, 100044 Beijing, PR China

^b Institute of Chemistry, Chinese Academy of Sciences, 100190 Beijing, PR China

*Email: dkjian@bjtu.edu.cn *Email: wsong@iccas.ac.cn

Experimental

Electrochemical Measurements: Rotating disk electrode (RDE) measurements were carried at a rate of 10 mV s⁻¹ with varying rotating speed from 625 to 2500 rpm on ALS RRDE-3A instrument. Koutecky–Levich plots (J^{-1} vs. $\omega^{-1/2}$) were analyzed at various electrode potentials, in which the slopes of linear fit lines were used to calculate the number of electrons transferred (n) on the basis of the Koutecky-Levich equation:¹

$$\frac{1}{J} = \frac{1}{J_k} + \frac{1}{J_L} = \frac{1}{J_k} + \frac{1}{B\omega^{1/2}}$$

$$B = 0.62nFC_0(D_0)^{2/3}\nu^{-1/6}$$

Where J is the measured current density, and J_K and J_L are the kinetic- and diffusion limiting current densities, ω is the angular velocity, n is transferred electron number, F is the Faraday constant (96485 C mol⁻¹), C_0 is the bulk concentration of O₂ (1.26 × 10⁻⁶ mol cm⁻³), D_0 is the diffusion coefficient of O₂ (1.93 × 10⁻⁵ cm² s⁻¹), and ν is the kinematic viscosity of the electrolyte (1.09 × 10⁻² cm² s⁻¹). For Tafel plots, the kinetic current was calculated from the mass-transport correction of RDE curves according to:¹

$$J_k = \frac{J_L \times J}{J - J_L}$$

For the Rotating ring-disk electrode (RRDE) measurements, 15 ug catalyst was loaded on the RRED of a disk GCE (4 mm in diameter) and Ag ring electrode (5 mm inner diameter and 7 mm outer diameter). The cathodic scanning was the same as RDE's measurements, and the ring potential was constant at 1.5 V vs RHE. The percentage of HO₂⁻ ($P_{HO_2^-}$) and the electron transfer number (n) was determined by the followed equations:²

$$P_{HO_2^-} = 200 \times \left(1 - \frac{I_D}{I_D + I_R/E_f}\right)$$

$$n = 4 \times \frac{I_D}{I_D + I_R/E_f}$$

Where I_D and I_R were the disk and ring current respectively, and E_f is current collection efficiency of the Ag ring which was 0.424.

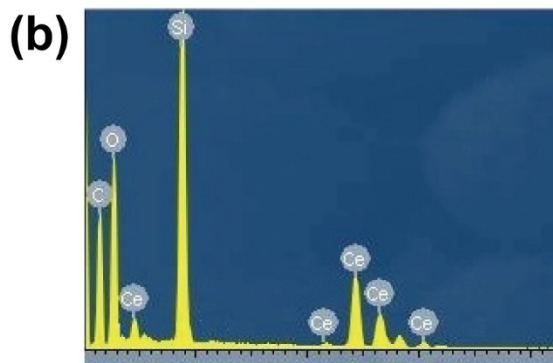
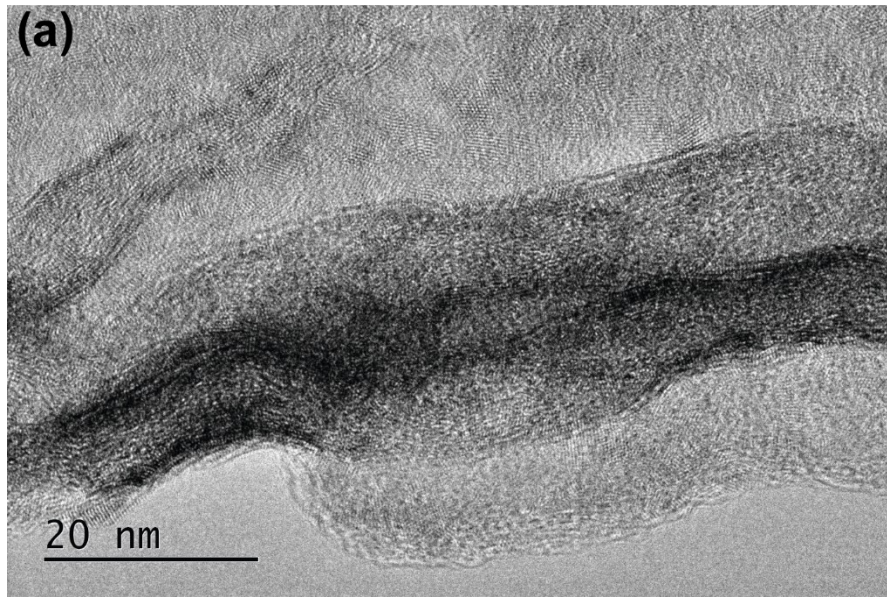


Figure S1. (a) A large area of SEM image of CeGS with lattice fringes almost full of the graphene nanosheet. (d) EDS spectra of CeGS.

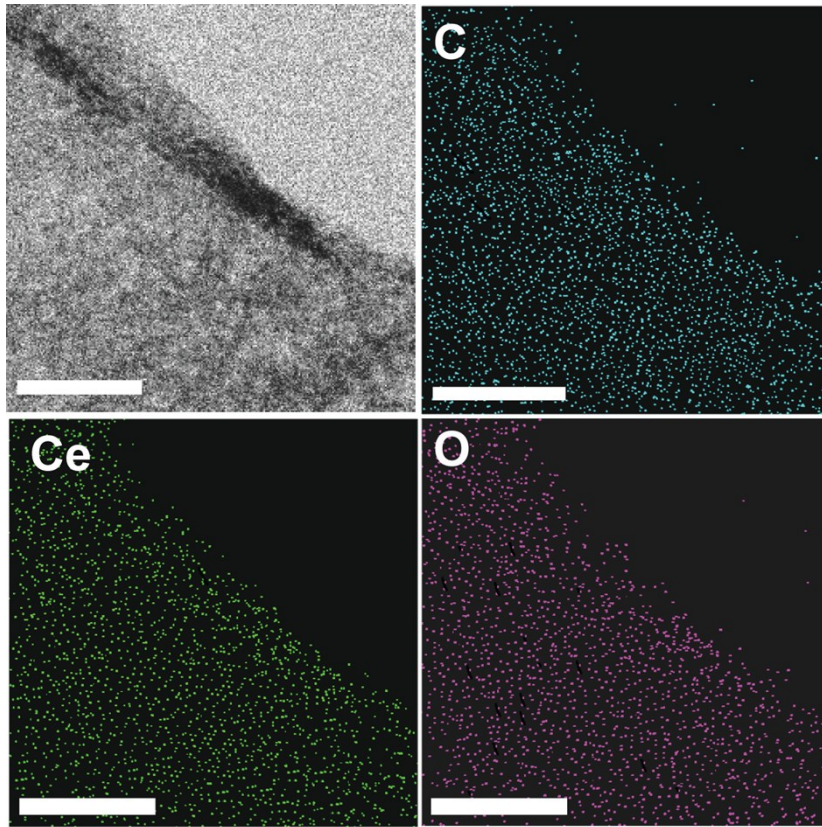


Figure S2. The elements distribution mapping images of CeGS. The scale bar is 100 nm.

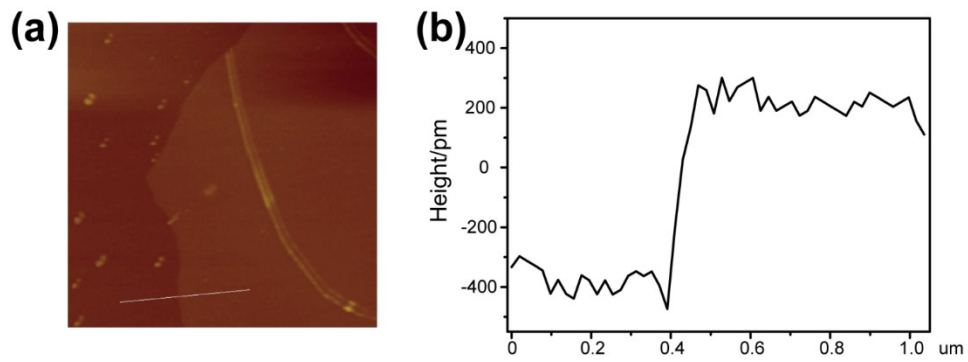


Figure S3. (a) AFM image and (b) height profile of GO.

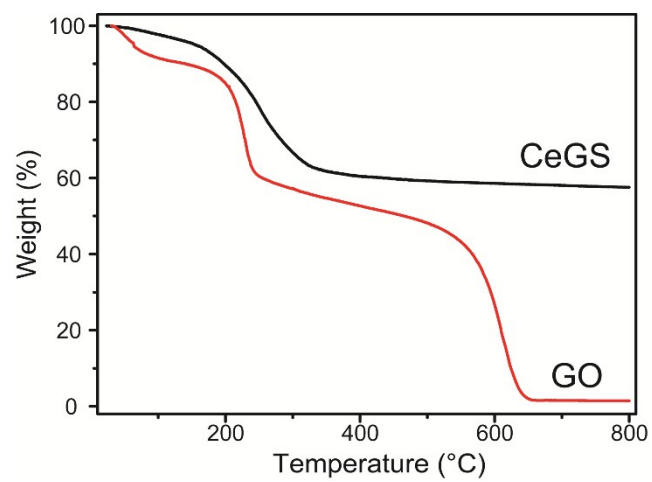


Figure S4. Thermal gravimetric analysis (TGA) curves of CeGS and pristine GO.

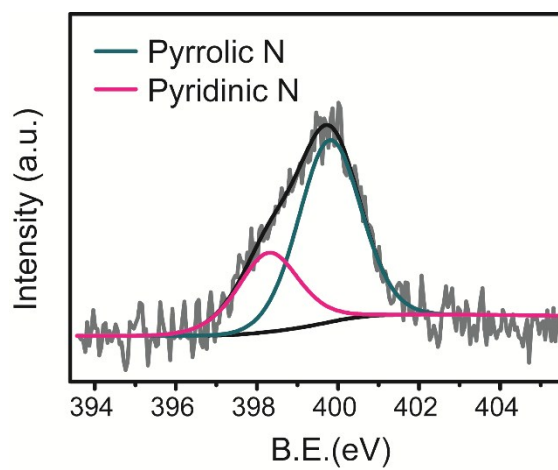


Figure S5. N 1s XPS spectra of CeGS

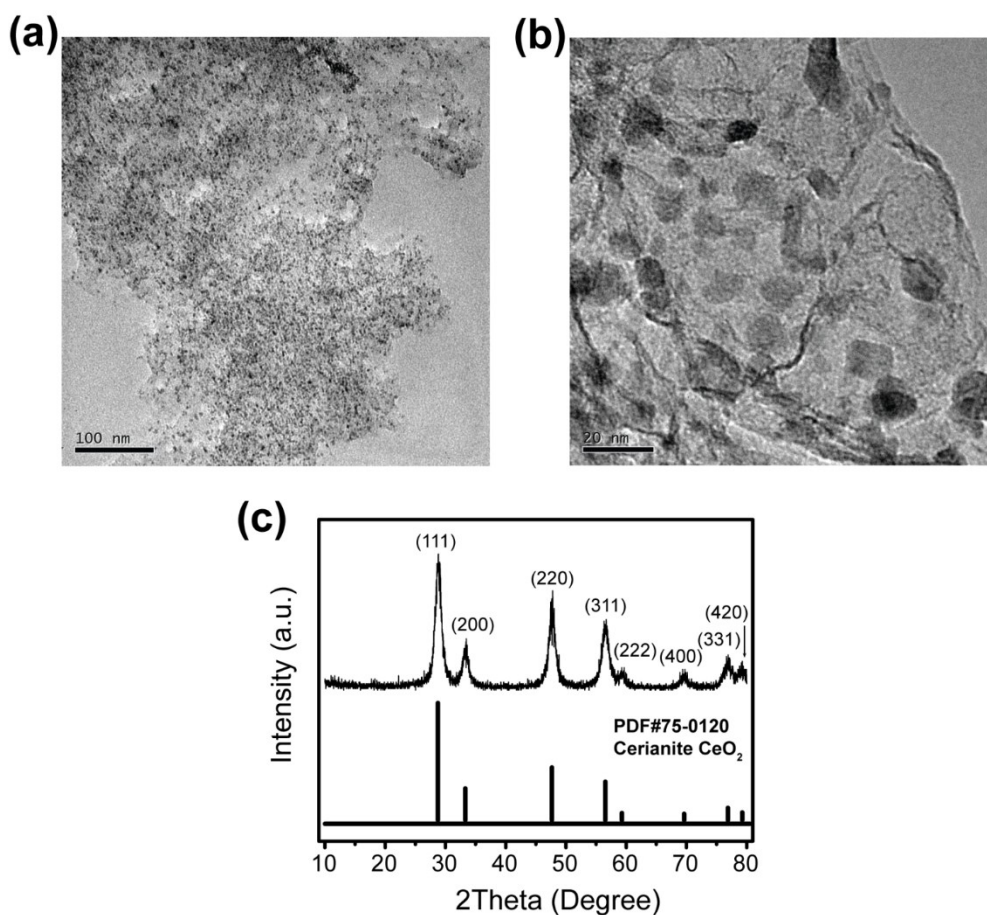


Figure S6. (a) Low, (b) high resolution TEM images and (c) XRD pattern of CeGN

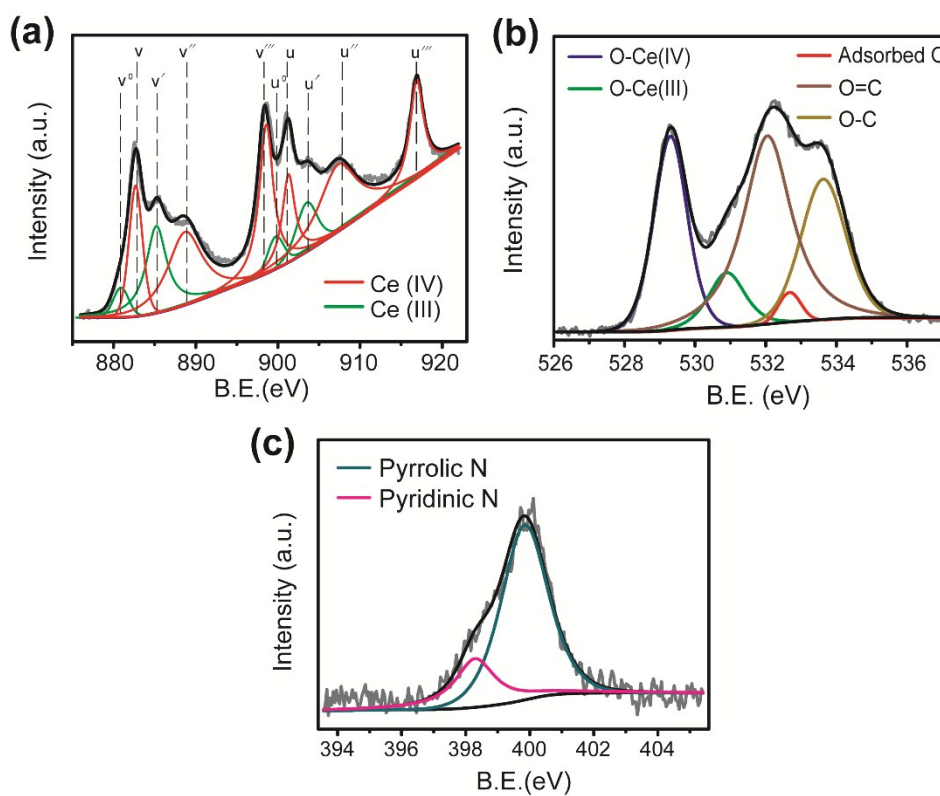


Figure S7. (a) Ce 3d, (b) O 1s and (c) N 1s XPS spectra of CeGN.

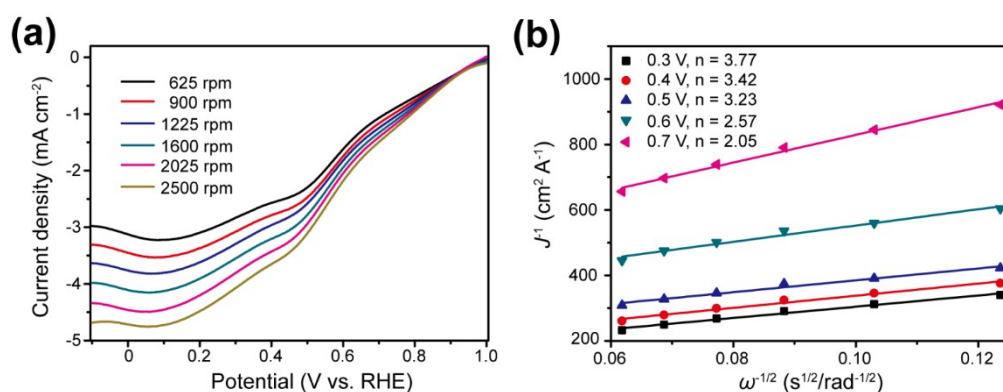


Figure S8. (a) RDE voltammograms of CeGN in O_2 -saturated 0.1 M KOH at various rotation speed at a scan rate of 10 mV s^{-1} , (b) Koutecky-Levich plots of CeGN at different potentials derived from RDE measurements.

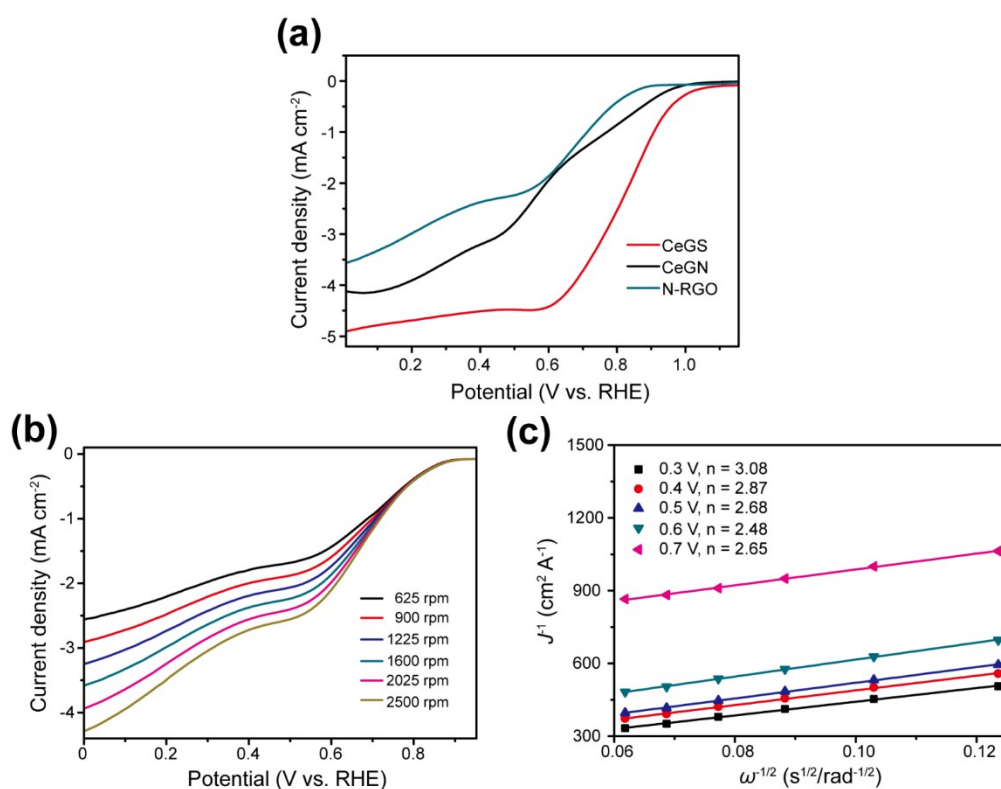


Figure S9. (a) RDE voltammograms of CeGS, CeGN and N-RGO in O_2 -saturated 0.1 M KOH with a sweep rate of 10 mV s^{-1} at 1600 rpm, (b) RDE voltammograms of N-RGO in O_2 -saturated 0.1 M KOH at various rotation speed, (c) Koutecky-Levich plots of N-RGO at different potentials derived from RDE measurements.

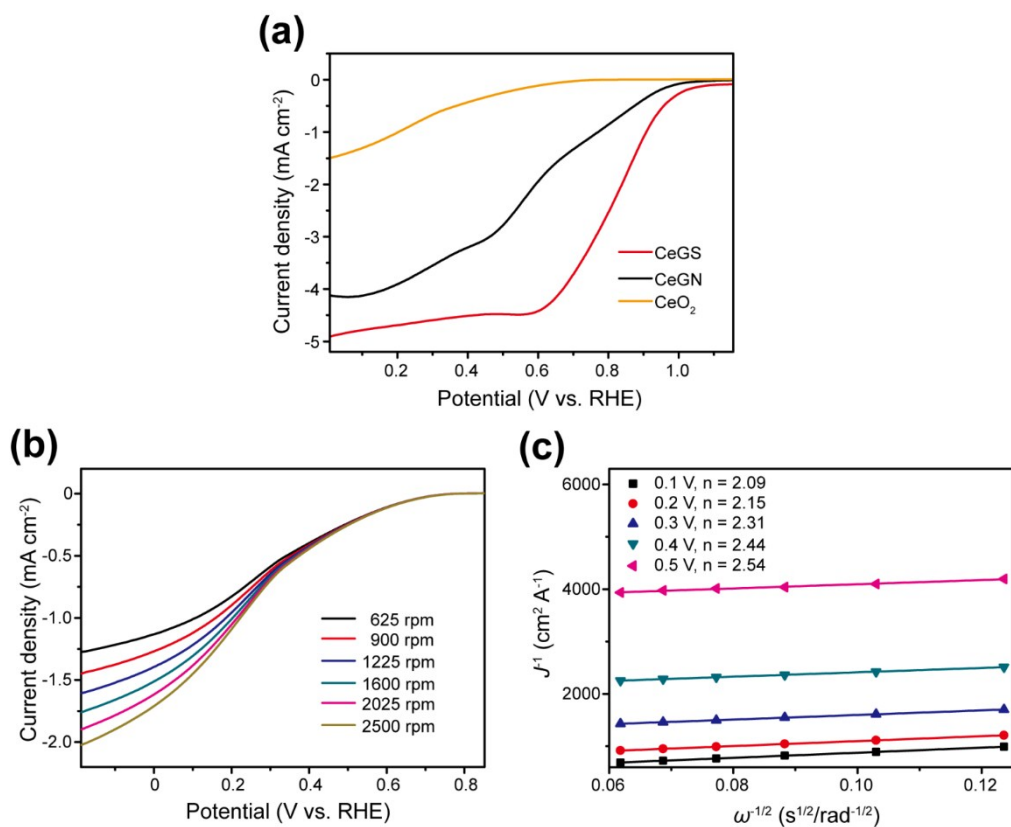


Figure S10. (a) RDE voltammograms of CeGS, CeGN and CeO₂ in O₂-saturated 0.1 M KOH, (b) RDE voltammograms of CeO₂ at various rotation speed, (c) Koutecky-Levich plots of CeO₂ at different potentials.

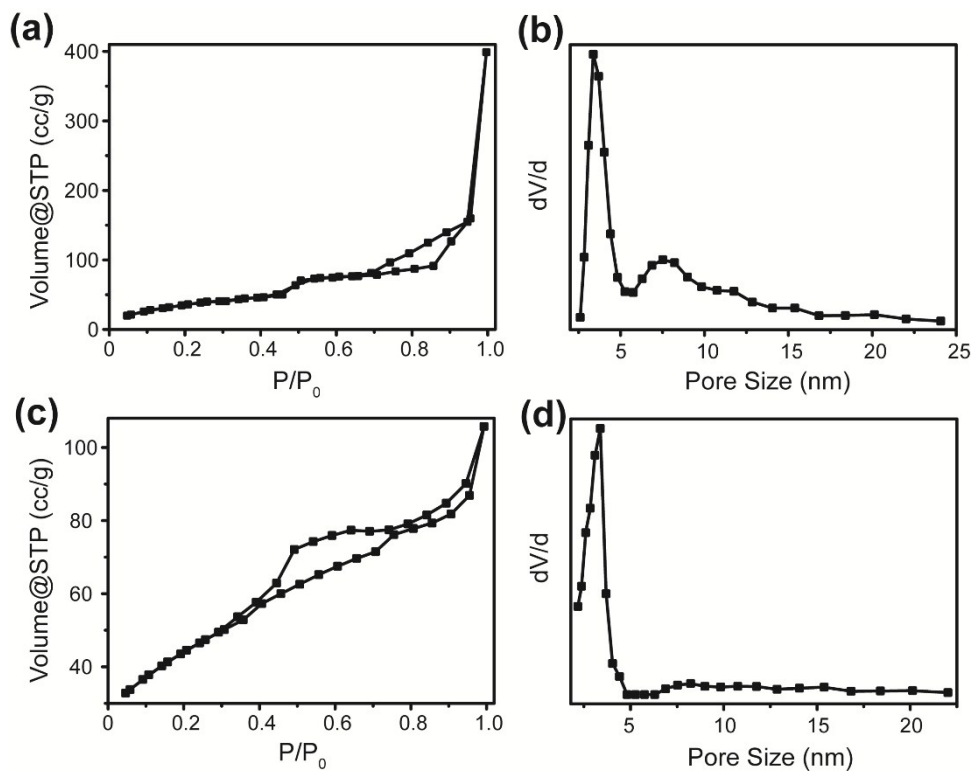


Figure S11. (a, c) N₂ adsorption-desorption isotherm curve and (b, d) pore size distributions of CeGS (a, b) and CeGN (c, d)

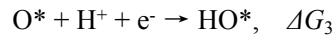
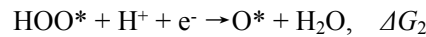
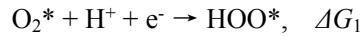
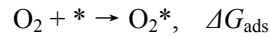
Theoretical calculation

All calculations were carried out within the scheme of periodic DFT+U, using the Vienna ab initio simulation package (VASP). The projector augmented wave (PAW) method was employed for the exchange-correlation term, by the generalized gradient approximation (GGA) using the Perdew-Wang (PW91) functional,³ and with the cut-off energy of 400 eV, total energy convergence of 1×10^{-4} eV and force convergence of 0.01 eV Å⁻¹. Hubbard U correction was adopted to minish the error caused by f electrons of Ce element, in which the LDAUU parameter was fixed at 0.5. (111) facet was representatively chosen to survey the surface chemical process in ORR, since it was the most stable facet in the cubic fluorite CeO₂ crystals during the several highly probable low-index surfaces.⁴ For both the two catalyst, a slab model of six-layer (111) surface-exposed super-cell with the lattice parameters of 11.5 × 11.5 Å was adopted, with a vacuum spacing of 20.0 Å above the top O layer. The numbers of Ce and O in the control sample (CeGN) were 18 and 36 respectively, obeying stoichiometric ratio. In order to simplify the calculation, only the single oxygen vacancy (V_O) was considered, and it was only placed in the top O layer in the constructing of CeGS surface. The schematics of the two adjusted surfaces were displayed in Figure S12. All the intermediates and top-three atom layers in catalysts were relaxed during the calculation, while the unrelaxed layers were set according to the results of bulk relaxation. (6×6×1) Monkhorst – Pack mesh k-points was used through all the steps, to guarantee the sufficient accuracy of the results. From the previous DFT studies,⁴ the magnetic effect for CeO₂ by spin-polarization calculations is insignificant for adsorption energies (ΔE_{ads}) and geometries. So we conducted the surface calculations with non-spin-polarization methods, just except bare CeO₂ surface and isolated oxygen molecule. The free energy changes of elementary reactions were adjusted *versus* the reversible hydrogen electrode (RHE) scheme proposed by Nørskov et al.⁵

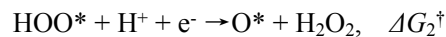
The equation associated with ΔE_{ads} was interpreted as:

$$\Delta E_{\text{ads}} = E_{\text{slab} + \text{O}_2} - E_{\text{slab}} - E_{\text{O}_2}$$

where $E_{\text{slab} + \text{O}_2}$, E_{slab} , and E_{O_2} were the calculated energies of O₂-adsorbed CeO₂ surface, bare CeO₂ surface, and a triplet gas-phase spin-polarized oxygen molecule, respectively. After the adsorption of O₂, another four elementary reactions based on the mechanism of peroxy intermediates involving the catalysts was delineated to investigate the whole reaction pathways. All the elementary reactions were exhibited as below:



Sometimes, a two-electronic oxygen reduction pathway accompanied with the generation of H₂O₂ may happen in ORR, in which the first two steps kept the same but the following elementary reaction took place as:



The gibbs free energy (ΔG) was calculated by correcting the DFT energies for zero point energies and entropy *via*

$$\Delta G = \Delta E + \Delta ZPE - T\Delta S$$

Where ΔE and ΔZPE were the changes in DFT energy and zero-point energy of the adsorbates both obtained by calculation, while ΔS presented approximately the loss of entropy of the gas phase molecules upon binding them to the surface.⁶

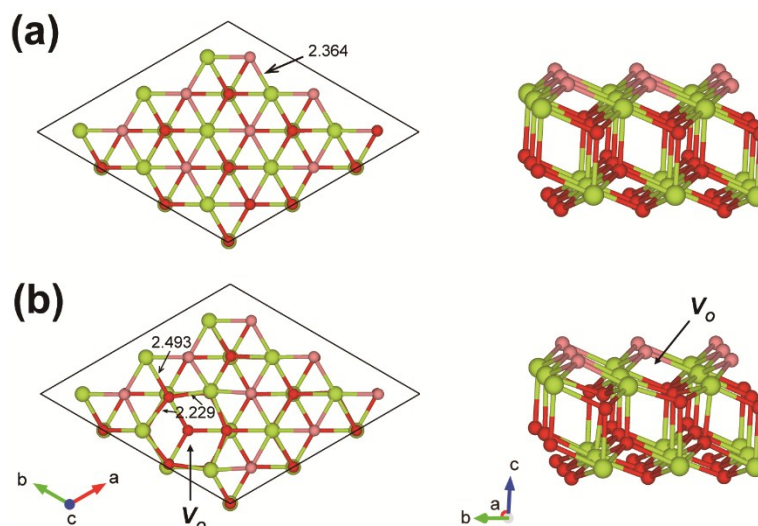


Figure S12. The slab models of six-layer (111) surface-exposed super-cell with the lattice parameters of $11.5 \times 11.5 \text{ \AA}$, which were used to simulate the surfaces of CeGS (a) and CeGN (b). The yellow, red and pink balls were representative for Ce, under-layer O and top-layer O atoms respectively. The left and right images were along the c (top-view) and a axis (side-view) respectively.

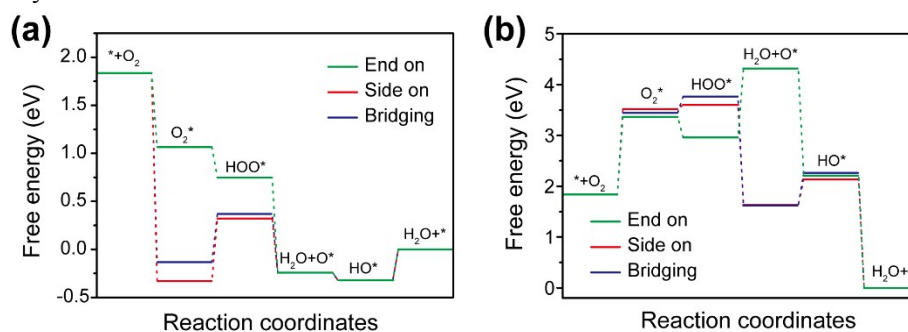


Figure S13. Schematic diagram of ΔG of elementary reactions for ORR on V_o - CeO_2 -111 (a) and CeO_2 -111 (b) at 0 V (RHE) in all the three adsorption pathways.

Table S1. The data of ΔG of elementary reactions in all the three adsorption pathways.

		ΔG_{ads}	ΔG_1	ΔG_2	ΔG_3	ΔG_4
V_o-CeO_2-111	end-on	-0.772	-0.317	-0.988		
	side-on	-2.166	0.650	-0.562	-0.082	0.322
	bridging	-1.969	0.504	-0.612		
CeO_2-111	end-on	1.526	-0.404	1.36	-2.104	-2.215
	side-on	1.68	0.085	-1.97	0.507	-2.139
	bridging	1.609	0.319	-2.146	0.644	-2.263

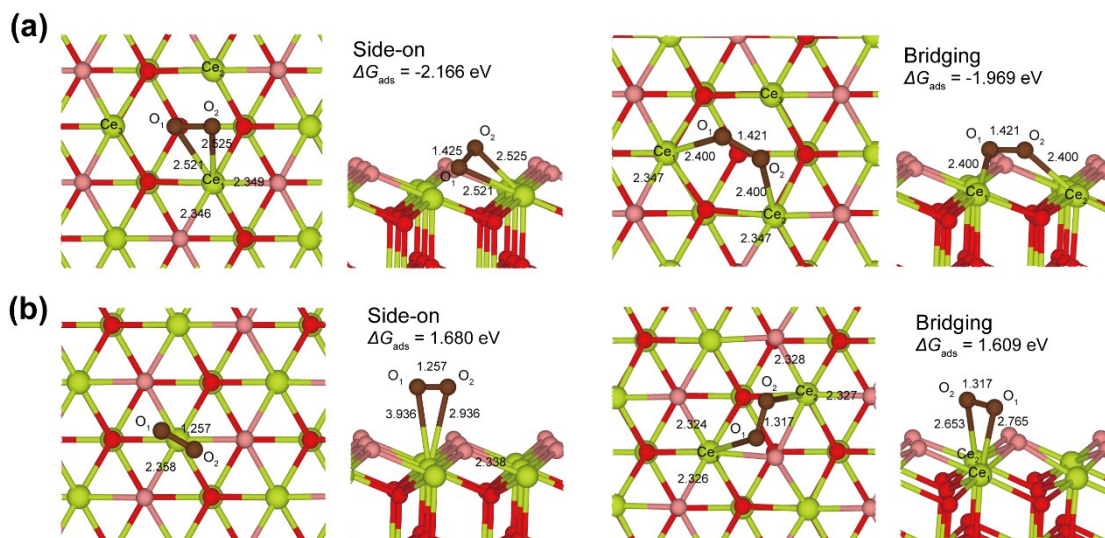


Figure S14. The side-on (left) and bridging (right) adsorption configurations of O₂ on V₀-CeO₂-111 (a) and CeO₂-111 (b) from top-view and side-view. The yellow, red, pink and brown balls were representative for Ce, under-layer O, top-layer O, and adsorbed O atoms respectively.

Table S2. The bond distances in the intermediates and with catalysts in the pathways on V₀-CeO₂-111 and CeO₂-111. The unit is Å.

		O ₂ *			HOO*			O*	HO*
		Ce-O1	Ce-O2	O-O	Ce-O1	Ce-O2	O-O	Ce-O	Ce-O
V ₀ -CeO ₂ -111	end-on	2.366	2.379	1.422	3.630	2.504	1.462		
		2.521	2.525		2.589	2.898			
	side-on	2.521 ^a	2.525 ^a	1.425	2.595 ^a	2.908 ^a	1.477	2.323	2.662
		2.370 ^b			2.558 ^b				
	bridging	2.400	2.400 ^a		2.540	2.624 ^a			
		2.511 ^b	2.511 ^b	1.421	2.499 ^b	3.562 ^b	1.474		
V ₀ -CeO ₂ -111	end-on	2.910	3.900	1.242	2.504	3.213	1.318	2.207	2.318
	side-on	2.936	2.936	1.257	2.826	2.879	1.379	2.313	2.380
	bridging	2.765	2.653 ^a	1.317	2.932	3.050 ^a	1.462	2.332	2.656

^a refers to the bond distances of O with Ce₂ in Figure S12

^b refers to the bond distances of O with Ce₃ in Figure S12

Table S3. The Bader charge polarizations (*e*⁻) in the intermediates in the pathways on V₀-CeO₂-111 and CeO₂-111.

		O ₂ *			HOO*		O*	HO*	
		O1	O2	O1	O2	H	O	O	H
V ₀ -CeO ₂ -111	end-on	-0.586	-0.394	-0.681	-0.611	0.598			
	side-on	-0.686	-0.502	-0.684	-0.654	0.618	-1.176	-1.307	0.586
	bridging	-0.580	-0.560	-0.665	-0.691	0.644			
CeO ₂ -111	end-on	-0.078	0.006	-0.277	-0.339	0.615	-0.483	-0.993	0.602

side-on	-0.042	-0.099	-0.264	-0.512	0.626	-0.464	-0.940	0.615
bridging	-0.069	-0.131	-0.068	-0.603	0.613	-0.466	-0.729	0.689

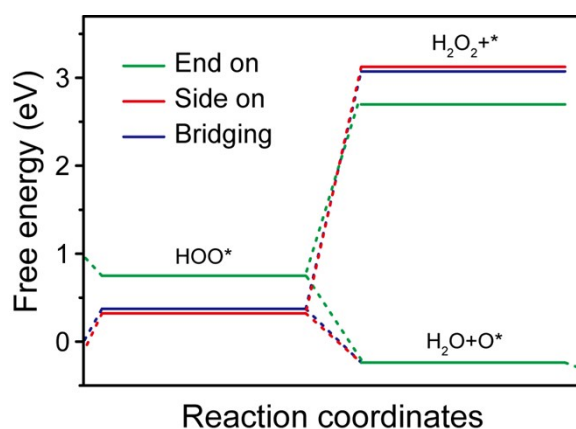


Figure S15. Schematic diagram of ΔG of the third elementary reaction in four and two electrons pathways on V_O - CeO_2 -111.

Table S4. The data of ΔG of the following elementary reactions after the formation of HOO^* in four and two electrons pathways respectively on V_O - CeO_2 -111.

	ΔG_2	ΔG_2^\ddagger
end-on	-0.988	2.699
side-on	-0.562	3.125
bridging	-0.612	3.075

Reference

1. a) A. J. Bard and L. R. Faulkner, *Electrochemical Methods, 2nd ed.*; Wiley: New York, 2001; b) D. R. Lawson, L. D. Whiteley, C. R. Martin, M. N. Szentirmay and J. I. Song, *J. Electrochem. Soc.*, 1988, **135**, 2247-2253.
2. U. A. Paulus, T. J. Schmidt, H. A. Gasteiger and R. J. Behm, *J. Electroanal. Chem.*, 2001, **495**, 134-145.
3. a) G. Kresse and J. Hafner, *Phys. Rev. B*, 1993, **47**, 558-561; b) G. Kresse and J. Furthmüller, *Phys. Rev. B*, 1996, **54**, 11169-11186.
4. a) M. Baudin, M. Wójcik and K. Hermansson, *Surf. Sci.*, 2000, **468**, 51-61; b) Z. Yang, T. K. Woo, M. Baudin and K. Hermansson, *J. Chem. Phys.*, 2004, **120**, 7741-7749.
5. J. K. Nørskov, J. Rossmeisl, A. Logadottir, L. Lindqvist, J. R. Kitchin, T. Bligaard and H. Jónsson, *J. Phys. Chem. B*, 2004, **108**, 17886-17892.
6. a) H. A. Hansen, J. Rossmeisl and J. K. Nørskov, *Phys. Chem. Chem. Phys.*, 2008, **10**, 3722-3730; b) G. Baysinger, National Institute of Standards and Technology, 2015.